The Impact of Prediction Errors in the Domestic Peak Power Demand Management

.

Abstract--**In this paper, the impact of prediction errors on the performance of a domestic power demand management is thoroughly investigated. Initially, a real-time peak power demand management system using battery energy storage systems (BESSs), electric vehicles (EVs) and photovoltaics (PV) systems is designed and modeled. The model uses real-time load demand of consumers and their roof-top PV power generation capability, and the charging-discharging constraints of BESSs and EVs to provide a coordinated response for peak power demand management. Afterwards, this real-time power demand management system is modeled using autoregressive moving average and artificial neural networks-based prediction techniques. The predicted values are used to provide a day-ahead peak power demand management decision. However, any significant error in the prediction process results in an incorrect energy sharing by the energy management system. In this research, two different customers connected to a real power distribution network with realistic load pattern and uncertainty are used to investigate the impact of this prediction error on the efficacy of an energy management system. The study shows that in some cases the prediction error can be more than 300 percent. The average capacity of energy support due to this prediction error can go up to 0.9 kWh, which increases battery charging-discharging cycles, hence reducing battery life and increasing energy cost. It also investigates a possible relationship between environmental conditions (solar insolation, temperature and humidity) and consumers' power demand. Considering the weather conditions, a day-ahead uncertainty detection technique is proposed for providing an improved power demand management.**

Index Terms--ANN, ARMA, energy management loss, peak load shaving, power demand management, prediction error.

I. Introduction

THE traditional power grid was designed considering a unidirectional power flow from power stations to customers. The power stations were centralized and bulky and connected to the customer through long transmission lines [1]. In recent years, this traditional power system is experiencing a significant paradigm shift towards a smarter, automated and distributed system [1], [2]. There is an influx of small-scale and aggregated renewable energy sources such as solar, wind and biomass that are integrated into the grid. However, most of these renewable energy sources are intermittent, and their distributed placement creates power management challenges for utilities, for example, the control of power flow and maintenance of standard voltage and frequency limits and power system stability [1], [2].

With the pace of renewable energy penetration, new types of loads, e.g. electric vehicles (EVs) are also being integrated into the power systems. Although EVs have energy storage capability, their mobility makes them significantly different than the fixed installation of BESSs [3], [4]. The uneven distribution of EVs and the challenges due to their unregulated charging-discharging can be reversed as an opportunity through a coordinated demand management system. The bidirectional vehicle-to-grid (V2G) energy transfer from a single EV at home or aggregated EVs in a parking lot can provide various load and ancillary support to grids [3], [5]. Subsequently, a combination of EVs and fixed battery storage can minimize the uncertainty of vehicle's availability and intermittency of PVs. These energy storages can be charged during off-peak hours (periods of low electricity price) and discharge during peak load hours (periods of high electricity price) to reduce the energy usage cost. As the load profile of customers has increasing peaks overtime, the power system components (transmission lines, transformer, protection circuitry) needs to strengthen to manage this overcapacity [3]–[5]. A coordinated power demand management can reduce the peaks, which helps customers to reduce energy costs, and utilities to properly utilize their systems. Sometimes this coordinated demand management is realized using various day-ahead energy resources scheduling and optimization techniques or using various forecasting techniques [6]. The forecasting techniques are used to predict the load demand of consumers and their renewable energy generation capability (e.g. roof-top PV power generation) considering weather conditions to minimize the consumers' electricity costs [7]. Sometimes, energy price forecasting is also used to economically charge-discharge battery storage and EVs to reduce electricity consumption during high price [8]. These day-ahead power demand, generation, and electricity price forecasting help to effectively manage the cost-effective real-time operation of domestic appliances and the cycling of energy resources. However, any forecasting errors may substantially affect the operation of controllable resources and impact negatively to their cost-effective real-time operation. Therefore, this study aims to uncover the impact of prediction errors to the domestic peak power demand management and quantify them.

A significant and growing body of literature [9]–[11] has investigated the smart grid distribution-side demand management. Various combination of energy resources such as roof-top PVs [10], EVs and battery energy storage systems [3], [4], [11] are used for peak power demand management. In [12], [13], PVs and BESSs are used for peak shaving and power quality regulation. Authors in [14], [15] use a PV-based EV

charge management system to minimize their demands on the grid. Several studies [16], [17] have applied the load shifting techniques for managing distributed energy resources and minimizing electricity costs. Few authors [18] used energy resource scheduling and optimization techniques for domestic power demand management. Some authors [19] used real-time load and ancillary support systems. Various forecasting techniques such as artificial neural networks, wavelet neural networks, time series, fuzzy logic, and support vector machine are used for many power systems studies [20], [21]. The studies are limited to the short-term [22] and long-term [23] load forecasting for power system planning and operation, electricity price and energy market behavior forecasting [8], [24], and hourly or day-ahead renewable energy forecast [7], [25] to manage the available power generation. However, there is a little-published data that investigated the impact of these prediction errors on the domestic peak power demand management. Considering the previous research gaps, this paper aims to explore the consequences of prediction errors and their techniques on energy management. There are several areas where this study makes an original contribution such as

- modeling a real-time peak power demand management system using PVs, EVs and battery energy storage systems;
- designing and implementing a peak power demand management system using artificial neural networks (ANN) and autoregressive moving average (ARMA)-based prediction techniques;
- conducting a comparative study of the performance of ANN and ARMA in the peak power demand management;
- analyzing the impact of prediction errors on the performance of a domestic energy management systems;
- investigating the effect of prediction errors on the performance of battery energy storage systems and quantifying them; and
- defining a relationship between power demand, temperature, humidity and solar insolation, based on the environmental parameters, leading to the development of day-ahead uncertainty detection technique and an intelligent boundary setpoints determination technique for better demand management.

II. Related Previous Studies

A large number of authors utilized various forecasting techniques in several power system applications and research objectives. The most common forecasting techniques include time-series models, wavelet neural networks, regression methods, neural networks model, fuzzy logic, expert systems, and support vector machines (SVM) [20], [21], [26]. The time-series models are comprised of various approaches such as autoregressive moving average (a combination of autoregressive and moving average models), autoregressive moving average with exogenous variables, autoregressive integrated moving average and autoregressive integrated moving average with exogenous variables [20], [21], [26]. These techniques are applied in both short-term and long-term forecasting for control decisions, planning and management purposes [7], [8], [23]. The short-term forecasting, which is usually day-ahead, hourly or half-hourly, is applied to predict the consumers power demand, local renewable energy generation capability (roof-top PVs and wind power generation) identification, electricity dispatch and generator capacity scheduling, spinning reserve calculations, and used as an operational signal for energy management devices and information to utilities for reliability assessment [8], [22], [23], [27]. The long-term forecasting, which is usually weekly, monthly, half-yearly or yearly, is applied for the planning and expansion decision such as generator maintenance, network expansion, electricity price and energy market behaviour analysis [7], [22], [23], [26], [27]. The forecasting techniques applied to the customer-side perform the domestic load management, load shifting and day-ahead energy management [28]–[31]. However, little attention is paid to the use of forecasting techniques for peak load management using customers' available energy resources. Although some of the authors considered the amount of prediction errors while applying the prediction techniques to their objectives, there has been no detailed investigation to quantify these percentage of errors in terms of energy loss, i.e. the kWh battery power loss due to wrong cycling of battery storage. Considering these research gaps, this paper aims to explore the consequences of prediction errors and their techniques on energy management.

III. Prediction Techniques

A. Autoregressive Moving Average

An autoregressive moving average (ARMA) based technique ($ARMA(m,n)$) is the combination of two models, i.e., autoregressive $AR(m)$ and moving average $MA(n)$ model. The $AR(m)$ model includes the future values of its variables (maintaining a linear combination of its past observations), a constant, and a random error, and is given as:

$$\begin{aligned} y_t &= \sum_{i=1}^{m} \emptyset_i y_{t-i} + \zeta_t + \mathcal{C} \\ &= \emptyset_1 y_{t-1} + \emptyset_2 y_{t-2} + \cdots + \emptyset_m y_{t-m} + \zeta_t \\ &\quad + \mathcal{C} \end{aligned} \tag{1}$$

where ζ_t is the random error, $\mathcal{C}$ is a constant, $\emptyset_i$ are model parameters, m is the order of the model. On the other hand, moving average $MA(n)$ model uses the past errors to predict future values, and modeled as:

$$\begin{aligned} y_t &= \sum_{j=1}^{n} \partial_j \zeta_{t-j} + \zeta_t + \mathcal{D} \\ &= \partial_1 \zeta_{t-1} + \partial_2 \zeta_{t-2} + \cdots + \partial_n \zeta_{t-n} + \zeta_t \\ &\quad + \mathcal{D} \end{aligned} \tag{2}$$

where, n is used to define the order of the MA model, ∂_j is the model parameter, and the $\mathcal{D}$ is the mean of the series. The noise considered in the model is assumed to be a white noise having a constant variance and zero mean, and follows the typical normal distribution. The combination of the AR and MA model forms a $ARMA(m,n)$ time series, and can be represented as:

$$y_t = \sum_{i=1}^{m} \emptyset_i y_{t-i} + \zeta_t + \mathcal{C} + \sum_{j=1}^{n} \partial_j \zeta_{t-j} \tag{3}$$

In a manipulated expression ARMA model can be presented using lag or backshift operators, e.g. $Ly_t = y_{t-1}$. So, the ARMA model expression becomes

$$ARMA \quad \begin{cases} \zeta_t = \emptyset(L) y_t \ \ for\ AR(m) \\ y_t = \partial(L)\zeta_t \ for\ MA(n) \end{cases} \tag{4}$$

$$ARMA\ (m,n) \rightarrow \{\emptyset(L) y_t = \partial(L)\zeta_t$$

$$where\ \emptyset(L) = \left\{1 - \sum_{i=1}^{m} \emptyset_i L^i\right\}, \partial(L) = \left\{1 + \sum_{j=1}^{n} \partial_j L_j\right\} \tag{5}$$

The performance of the ARMA model while applied to predict the household power demand is shown in Figs 1 and 2. Two different household power demand is used to test the performance of ARMA prediction. The household power demand as shown in Fig. 1 is used to model the ARMA prediction technique and then, it is applied for a different time duration of the same house. The same model is used for a different household power demand in Fig. 2 to test its performance.

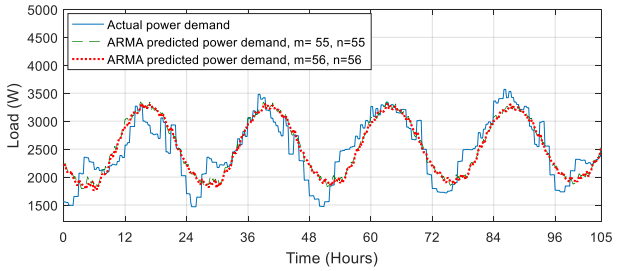

Fig. 1. ARMA-based consumer's load demand prediction performance (applied at house 1).

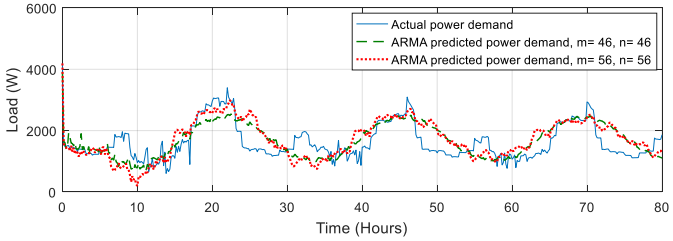

Fig. 2. ARMA-based consumer's load demand prediction performance (applied at house 2, which has a different load pattern and is unknown to initial modeling).

The order *(m, n)* of ARMA, has an impact on the prediction performance, as shown in (1-5. In Fig. 1, the orders 55 and 56 show a slight prediction variation. However, the variation is more evident in Fig. 2, where *m, n* are 46 and 56 respectively.

B. Artificial Neural Network

Artificial neural networks (ANN) is an alternate way to predict the time series in the domestic load curve. The ANN is self-adaptive, and data-driven that performs better for any nonlinear and complex data patterns unlike any traditional approaches. The architecture of the feed-forward neural network is shown in Fig. 3.

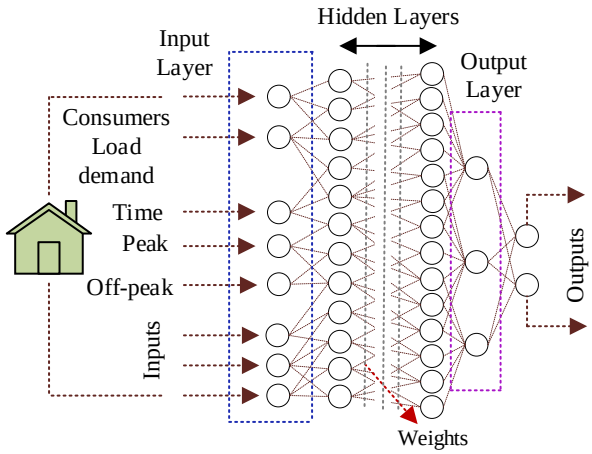

Fig. 3. A schematic of the feed forward neural networks.

The ANN has various hidden layers in between inputs and outputs. If the feed forward neural has g number of hidden layers, for the y_{t-i} $(i = 1, 2, \ldots, k)$ inputs to the hidden layers, the output (y_t) is expressed as:

$$y_t = \sum_{j=1}^{g} \delta_j f\left(\gamma_{0j} + \sum_{i=1}^{k} \gamma_{ij} y_{t-i}\right) + \delta_0 + \sigma_t, \forall t \tag{6}$$

where k is used to defined the number of inputs to the ANN, δ_0 is a bias term, the weights from/to hidden layers are defined using γ_{ij} $(i = 0, 1, 2, \ldots\ldots, k; j = 0, 1, 2, \ldots\ldots\ldots, g)$ and δ_j $(j = 0, 1, 2, \ldots\ldots, g)$, σ_t is a random shock, and γ_{0j} is a bias term. The $f(x) = \frac{1}{1+e^{-x}}$ in equation 6 is a logistic sigmoid function and used as a nonlinear activation function. The Gaussian, linear, or hyperbolic tangent functions can be an alternative of this nonlinear activation function. In case of the feed forward neural networks, it uses past observations to map nonlinear functions and generate a time series of its future values. For example, the predicted future value is given as:

$$y_t = f(y_{t-1}, y_{t-2}, y_{t-3}, \ldots\ldots, y_{t-k}, \mathcal{Z}) + \sigma_t \tag{7}$$

where, $\mathcal{Z}$ is the vector of all parameters. The function $f(x)$ is set based on the structure of the networks and the weights from/to hidden layers. A nonlinear least square method is used to determine the weights between the connections, and it functions of minimize the value of error function. If ϖ is denoted as the space of all connection weights, the minimization error function will be

$$F(\varpi) = \sum_{t} e_t^2 \tag{8}$$

$$F(\varpi) = \sum_{t} (y_t - \hat{y}_t)^2 \tag{9}$$

ANN-based consumer's load demand prediction performance is shown in Figs. 4 and 5. Alike ARMA, two different household power demand (H1 and H2) is used to test the ANN-based prediction performance under various scenario. The consumer's load demand (H1) in Fig. 4 is used to model the ANN prediction technique and then it is applied for a different time duration of the same house. The same model is used for a different household power demand (H2) in Fig. 5 to test its performance.

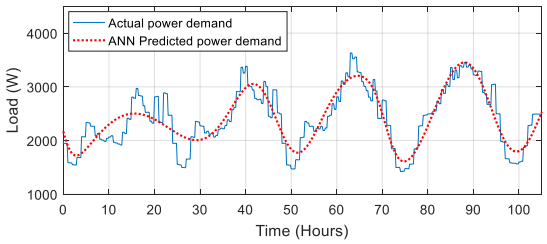

Fig. 4. ANN-based consumer's load demand prediction performance (applied at H1).

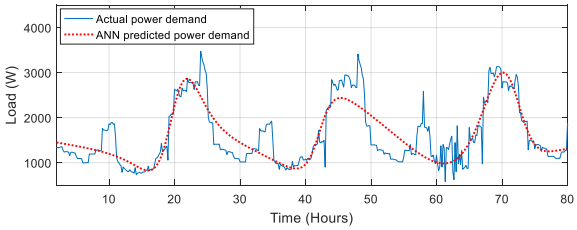

Fig. 5. ANN-based consumer's load demand prediction performance (applied at H2, which has a different load pattern and is unknown to initial modeling).

C. Prediction Performance During Uncertainty

In this section, the performance of ARMA and ANN-based prediction techniques under uncertainty is analyzed. Initially, uncertainty is added to the load curve of house 1 based on which the ARMA is modeled, as shown in Fig. 6. Afterwards, uncertainty is added to the second house, and the prediction performance is analyzed in Fig. 7. Like ARMA, ANN is also used to observe its performance during power demand uncertainty. From Figs. 6-8, it is clear that the performance of the ANN-based prediction is better than that of an ARMA-based prediction.

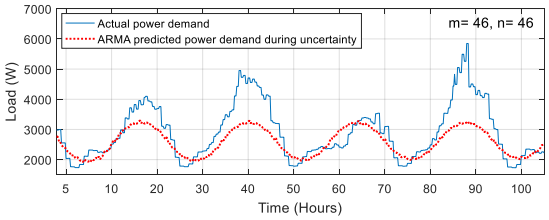

Fig. 6. Performance of the ARMA-based household power demand prediction during uncertainty at house 1 (based on which ARMA technique is modeled).

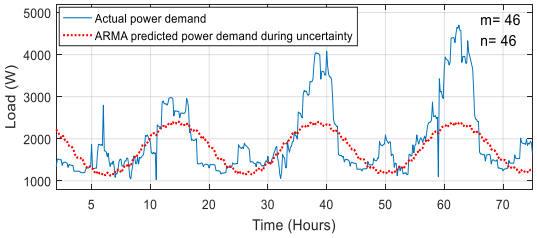

Fig. 7. ARMA-based consumer's load demand prediction performance during uncertainty (applied at house 2, which has a different load pattern).

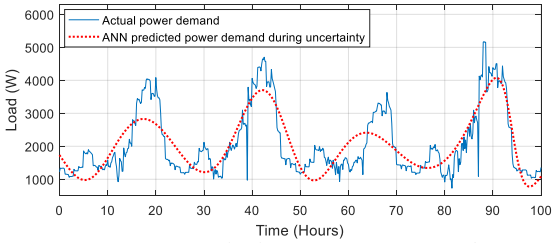

Fig. 8. ANN-based consumer's load demand prediction performance during uncertainty (applied at house 2, which has a different load pattern).

IV. Peak Power Demand Management

The proposed system consists of a BESSs, a vehicle-to-grid (V2G)-capable EV and a PV. A schematic of the system is shown in Fig. 9.

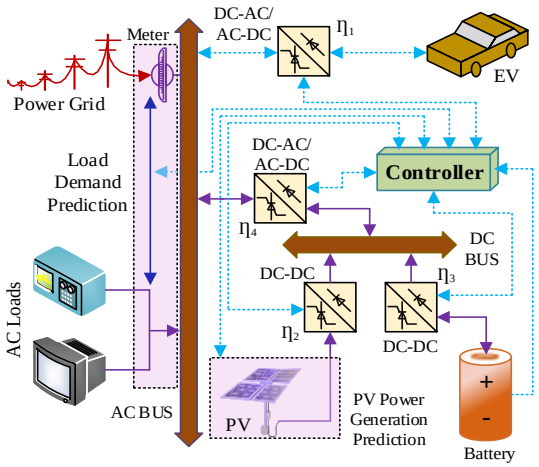

Fig. 9. Schematic of the proposed system.

The EV is plugged to the domestic AC bus (main bus of the house) using a V2G-capable charger. Basically, this charger is a bidirectional AC-DC/DC-AC converter (converter 1, as shown in Fig. 9). Another intermediate DC bus is used to integrate BESSs and PV unit using a bidirectional DC-DC converter (converter 3, as shown in Fig. 9) and a unidirectional DC-DC converter (converter 2), respectively. This intermediate DC bus is interconnected to the main bus (AC bus) using a bidirectional DC to AC and AC to DC converter. The controller reads the state-of-charge (SOC) of the battery and EV, PV power generation, and domestic power demand to manage the peak load condition through a controlled discharging and charging of EV and battery storage systems.

Consumers load demand and their roof-top PV power generation are predicted using ARMA and ANN-based techniques to manage their power demand day ahead of the actual operation. Based on these predicted values and some other parameter (e.g. battery and EV SOC and their charging-discharging boundaries, EV availability) peak load is managed. The performance of the PV power generation prediction during normal and uncertainty states are shown in Figs. 10 and 11 respectively.

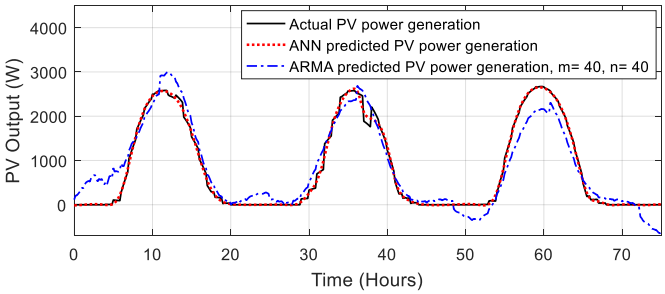

Fig. 10. The performance of the ARMA and ANN-based prediction for PV power generation under normal conditions.

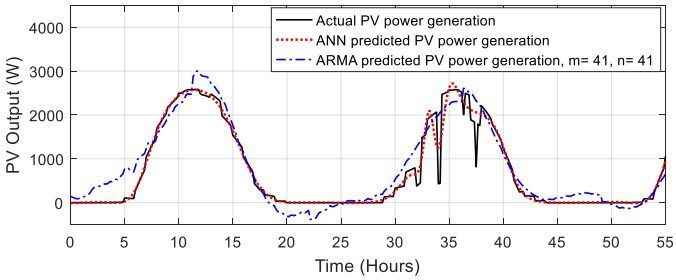

Fig. 11. The performance of the ARMA and ANN-based prediction for PV power generation during uncertainty.

Let us assume that the domestic power demand $(\mathfrak{D}_t^p)$ and the customers' desired base load demand $(\widehat{\mathfrak{D}}_t^p)$ are functions of power and time, and expressed as [19]:

$$\mathfrak{D}_t^p = f(p,t) \tag{10}$$

$$\widehat{\mathfrak{D}}_t^p = f(p_\tau,t) \tag{11}$$

The time (t) is the summation of both base-load (t_b) and peak load (t_p) periods and given as:

$$t = a\left(\sum_{t=t_b^s}^{t=t_b^e} t_b\right) + \mathscr{b}\left(\sum_{t=t_p^s}^{t=t_p^e} t_p\right) \tag{12}$$

where, t_b^s and t_p^s are the time when base load and peak load periods start. Likewise, t_b^e and t_p^e are the time when base and peak load periods end. a and $\mathscr{b}$ in equation 12 define the base and peak load occurrence frequency, respectively, for a particular time period. The off-peak (base load) and peak load periods are determined through a comparison with the customers' desired base load demand $(\widehat{\mathfrak{D}}_t^p)$, i.e.

$$\left(\mathfrak{D}_t^p - \widehat{\mathfrak{D}}_t^p\right)\begin{cases} +ve\ for\ peak\ load \\ -ve\ for\ off-peak \end{cases} \tag{13}$$

At $t^{th}\ (t \in t_b, t_p)$ time, if the power demand is $\mathfrak{D}_t^p > \widehat{\mathfrak{D}}_t^p$, the required power is supplied by the available energy resources, i.e. battery storage, PV, and EV will provide power to the common AC bus which are given as:

$$\mathcal{P}_r = \mathfrak{D}_t^p - \widehat{\mathfrak{D}}_t^p, \mathcal{P}_r > 0 \tag{14}$$

$$\mathcal{P}_r = \sum\left(\underbrace{\mathcal{P}_r^b}_{battery}, \underbrace{\mathcal{P}_r^{ev}}_{EV}, \underbrace{\mathcal{P}_r^{pv}}_{PV}\right) \tag{15}$$

where, $\mathcal{P}_r^b, \mathcal{P}_r^{ev}, \mathcal{P}_r^{pv}$ are the maximum available power from the BESSs, EV, and PV respectively. If the EV is not available, $\mathcal{P}_r^{ev} = 0$. If $\sum\left(\mathcal{P}_r^b, \mathcal{P}_r^{ev}, \mathcal{P}_r^{pv}\right) \neq \mathcal{P}_r$, the mismatch power, i.e. $\left\{\mathcal{P}_r - \sum\left(\mathcal{P}_r^b, \mathcal{P}_r^{ev}, \mathcal{P}_r^{pv}\right)\right\}$ is supplied by the grid. Let us assume the lower SOC boundary for EV and battery discharging are Θ_{ev}^{min}, and Θ_b^{min} respectively. If the SOC of EV and BESSs at $t^{th}\ (t \in t_b, t_p)$ time is Θ_{ev}^t and Θ_b^t, respectively, the maximum available power from EV and battery is written as:

$$\hat{\mathcal{P}}_r^{ev} = \{(\Theta_{ev}^t - \Theta_{ev}^{min}) * \Pi_c^{ev}\} * \eta_1 \quad for\ \Theta_{ev}^t > \Theta_{ev}^{min}, \hat{\mathcal{P}}_r^{ev} \in \mathcal{P}_r^{ev} \tag{16}$$

$$\hat{\mathcal{P}}_r^b = \left\{\left(\Theta_b^t - \Theta_b^{min}\right) * \Pi_c^b\right\} * \eta_3 * \eta_4 \quad for\ \Theta_b^t > \Theta_b^{min}, \hat{\mathcal{P}}_r^b \in \mathcal{P}_r^b \tag{17}$$

where, Π_c^{ev} and Π_c^b are the EV and battery storage capacity, respectively. η_1, η_3, η_4 are the efficiencies of the converter 1 (V2G-capable EV charger), converter 3 and converter 4, respectively.

At $t^{th}\ (t \in t_b, t_p)$ time, if the power demand is $\widehat{\mathfrak{D}}_t^p > \mathfrak{D}_t^p$, the energy storages (i.e. EV and battery storage) can charge from the available grid power $(\mathcal{P}_g)$ from the AC bus and it is given as:

$$\mathcal{P}_g = \widehat{\mathfrak{D}}_t^p - \mathfrak{D}_t^p, \mathcal{P}_g > 0 \tag{18}$$

This available grid power $(\mathcal{P}_g)$ will be divided among the battery storage and EV, i.e.

$$\mathcal{P}_g = \underbrace{\left\{\mathcal{P}_g^b - \mathcal{P}_{pv}\right\}}_{battery} + \underbrace{\mathcal{P}_g^{ev}}_{EV} \tag{19}$$

$$\mathcal{P}_{pv} = \mathcal{N} * \mathcal{P}_0^1 * \eta_2 \tag{20}$$

where, $\mathcal{P}_{pv}$ is the PV power generation, $\mathcal{P}_0^1$ is the output power from a single PV unit, $\mathcal{N}$ is the number of PV modules, η_2 is the efficiency of the converter 2. The required power to charge battery and EV in (19) depends on the SOC status and maximum charging limits. Let us assume that the maximum charging limits for battery and EV are Θ_b^{max}, and Θ_{ev}^{max} respectively. So, the maximum requested power by the battery and EV $(\hat{\mathcal{P}}_g^b)$ is given as:

$$\hat{\mathcal{P}}_g^b = \{(\Theta_b^{max} - \Theta_b^t) * \Pi_c^b\} * \eta_3 * \eta_4 \quad for\ \Theta_b^t < \Theta_b^{max}, \hat{\mathcal{P}}_g^b \in \mathcal{P}_g^b \tag{21}$$

$$\hat{\mathcal{P}}_g^{ev} = \{(\Theta_{ev}^{max} - \Theta_{ev}^t) * \Pi_c^{ev}\} * \eta_1 \quad for\ \Theta_{ev}^t < \Theta_b^{max}, \hat{\mathcal{P}}_g^{ev} \in \mathcal{P}_g^{ev} \tag{22}$$

where $\hat{\mathcal{P}}_g^b \in \mathcal{P}_g^b$ and $\hat{\mathcal{P}}_g^{ev} \in \mathcal{P}_g^{ev}$. Considering the charging-discharging strategies, the number of energy sources and loads connected to the main bus changes over the peak and off-peak load periods. The sources and loads connected to the main bus at a particular time is expressed as [19]:

$$Loads \begin{cases} \underbrace{\mathfrak{D}_t^p}_{power\ demand\ of\ appliances} \\ \underbrace{[\{(\Theta_b^{max} - \Theta_b^t) * \Pi_c^b\} * \eta_3 * \eta_4]}_{battery} \\ \underbrace{[\{(\Theta_{ev}^{max} - \Theta_{ev}^t) * \Pi_c^{ev}\} * \eta_1]}_{EV} \end{cases} for\ \mathfrak{D}_t^p < \widehat{\mathfrak{D}}_t^p \tag{23}$$

$$Sources \begin{cases} \underbrace{[\{(\Theta_b^t - \Theta_b^{min}) * \Pi_c^b\} * \eta_3 * \eta_4]}_{battery} \\ \underbrace{[\{(\Theta_{ev}^t - \Theta_{ev}^{min}) * \Pi_c^{ev}\} * \eta_1]}_{EV} \\ \underbrace{[\mathcal{N} * \mathcal{P}_0^1 * \eta_2]}_{PV} \end{cases} for\ \mathfrak{D}_t^p > \widehat{\mathfrak{D}}_t^p \tag{24}$$

The polarity of the power flow identifies the charging-discharging mode of the battery and EV. If the current flow from the battery, EV and PV are $i_{\mathscr{b}}, i_{ev} i_{pv}$, respectively, the equation becomes

$$\forall i \in f\left(l_t^p, t\right) = \begin{cases} i_{ev}, i_{\mathscr{b}} < 0\ for\ \mathfrak{D}_t^p > \widehat{\mathfrak{D}}_t^p \\ i_{ev}, i_{\mathscr{b}} > 0\ for\ \mathfrak{D}_t^p < \widehat{\mathfrak{D}}_t^p \\ i_{pv} = 0\ for\ \mathcal{P}_{pv} = 0 \\ i_{pv} > 0\ for\ \mathcal{P}_{pv} > 0 \end{cases} \tag{25}$$

The power demand management considering the real-time values of load curve, charging-discharging boundaries of battery and EV is illustrated in algorithm 1.

Algorithm 1: real-time power demand management

Acquire: power demand $\mathfrak{D}_t^p = f(p,t)$ and set the value $\widehat{\mathfrak{D}}_t^p$
while $\left(\mathfrak{D}_t^p < \widehat{\mathfrak{D}}_t^p\right)\{$
  calculate: the available power $\mathcal{P}_g$
  check: boundary conditions of battery storage $\Pi_c^b, \Theta_b^t, \Theta_b^{max}$ and calculate $\hat{\mathcal{P}}_g^b$
  check: availability of EV and its boundary conditions $\Pi_c^{ev}, \Theta_{ev}^t, \Theta_{ev}^{max}$ and calculate $\hat{\mathcal{P}}_g^{ev}$
  check: PV power generation $\mathcal{P}_{pv}$
  if $\mathcal{P}_{pv} > 0$
    calculate $(\mathcal{P}_g^b - \mathcal{P}_{pv})$ and divide $\mathcal{P}_g$ power to $\{\mathcal{P}_g^b - \mathcal{P}_{pv}\}$ and $\mathcal{P}_g^{ev}$
  elseif $\mathcal{P}_{pv} = 0$
    divide $\mathcal{P}_g$ power to $\mathcal{P}_g^b$ and $\mathcal{P}_g^{ev}$
    continue process and check condition in 2
while $\left(\mathfrak{D}_t^p > \widehat{\mathfrak{D}}_t^p\right)\{$
  calculate: the required load-support from sources $\mathcal{P}_r$
  check: PV power generation $\mathcal{P}_{pv}$
  if $\mathcal{P}_{pv} > \mathcal{P}_r$
    $\mathcal{P}_{pv} \rightarrow \mathcal{P}_r$
  elseif $\mathcal{P}_{pv} < \mathcal{P}_r$
    check: availability of EV and its boundary conditions $\Pi_c^{ev}, \Theta_{ev}^t, \Theta_{ev}^{min}$ and calculate $\hat{\mathcal{P}}_r^{ev}$
    if $\left(\mathcal{P}_{pv} + \hat{\mathcal{P}}_r^{ev}\right) > \mathcal{P}_r$
      $\left(\mathcal{P}_{pv} + \hat{\mathcal{P}}_r^{ev}\right) \rightarrow \mathcal{P}_r$
    else
      check: boundary conditions of battery storage $\Pi_c^b, \Theta_b^t, \Theta_b^{min}$ and calculate $\hat{\mathcal{P}}_r^b$
      $\mathcal{P}_r \rightarrow \sum\left(\mathcal{P}_r^b, \mathcal{P}_r^{ev}, \mathcal{P}_r^{pv}\right)$
      Continue the process and check the conditions in 2 and 12

Let us assume that the load demand of consumers and their PV power generation using ANN prediction (as shown in equations 6-7) are $\mathfrak{D}_{t,p}^{ann}$and $\mathcal{P}_{pv}^{ann}$, respectively. The error between the predicted and actual values in consumers load demand and their PV power generation capability is expressed as:

$$\lambda = \mathfrak{D}_t^p - \mathfrak{D}_{t,p}^{ann} \tag{26}$$

$$\Upsilon = \mathcal{P}_{pv} - \mathcal{P}_{pv}^{ann} \tag{27}$$

where, λ is the error in the power demand prediction and Υ is the error in PV power prediction. Based on this prediction value power demand management will be executed as described in algorithm 2.

Algorithm 2: power demand management with ANN prediction

1: **Initialization**: set the parameter of y_{t-i}, y_t, $\mathcal{P}_{pv}^{t-1}, \mathcal{P}_{pv}^t$, where $\left(\mathcal{P}_{pv}^{t-1}, \mathcal{P}_{pv}^t\right) \in \left\{\mathcal{P}_{pv} = \mathcal{N} * \mathcal{P}_0^1 * \eta_2\right\}$ and $(y_{t-i}, y_t) \in \mathfrak{D}_t^p$
2: set number of hidden layers and the training algorithm to the Bayesian Regularization.
3: train the feed forward neural networks for power demand with y_{t-i} and y_t data, where $y_t = f(p,t)$
4: train the feed forward neural networks for PV with $\mathcal{P}_{pv}^{t-1}$ and $\mathcal{P}_{pv}^t$
5: **Prediction**: get the predicted power demand y_t, $y_{t-i} \in \mathfrak{D}_{t,p}^{ann} = f(p,t)$ and set the value $\widehat{\mathfrak{D}}_t^p$
6: continue with algorithm 1: step 2- 5
7: **prediction**: PV power generation $\mathcal{P}_{pv}^t$
8: continue with $\mathcal{P}_{pv}^t$ with algorithm 1: step 7- 13
9: **prediction**: PV power generation $\mathcal{P}_{pv}^t$
10: continue with $\mathcal{P}_{pv}^t$ with algorithm 1: step 15-24

Let us assume that the load demand of customers and their PV power generation using ARMA prediction (as shown in equation 3) are $\mathfrak{D}_{t,p}^{arma}$and $\mathcal{P}_{pv}^{arma}$, respectively. The error between the predicted and actual values in load demand of consumers and their PV power generation is expressed as:

$$\alpha = \mathfrak{D}_t^p - \mathfrak{D}_{t,p}^{arma} \tag{28}$$

$$\beta = \mathcal{P}_{pv} - \mathcal{P}_{pv}^{arma} \tag{29}$$

where, α is the error in the power demand prediction and β is the error in PV power prediction. Based on this prediction value power demand management will be executed as described in algorithm 3.

Algorithm 3: power demand management with ARMA prediction

1: **Initialization**: set the parameter of y_{t-i}, y_t, $\mathcal{P}_{pv}^{t-1}, \mathcal{P}_{pv}^t$, where $\left(\mathcal{P}_{pv}^{t-1}, \mathcal{P}_{pv}^t\right) \in \left\{\mathcal{P}_{pv} = \mathcal{N} * \mathcal{P}_0^1 * \eta_2\right\}$
2: set the order, $AR(m)$ and $MA(m)$, $ARMA(m,n)$
3: set the y_{t-i} and $\mathcal{P}_{pv}^{t-1}$ to predict $\mathfrak{D}_{t,p}^{arma}$ and $\mathcal{P}_{pv}^{arma}$, where $\left(y_t, y_{t-i}, \mathfrak{D}_{t,p}^{arma}\right) \in \left\{\mathfrak{D}_t^p = f(p,t)\right\}$ and $\left(\mathcal{P}_{pv}^{t-1}, \mathcal{P}_{pv}^t, \mathcal{P}_{pv}^{arma}\right) \in \mathcal{P}_{pv}$
4: follow algorithm 2: step 5-10

V. Case Studies

In this section, various case studies using the proposed control algorithm are presented. The case studies are conducted based on a real Australian power network, located in Nelson Bay, NSW, Australia. This real network data is obtained from the 'Smart Grid, Smart City (SGSC)' database, maintained by Ausgrid [32], [33]. A single line diagram of the network is shown in Fig. 12 [32], [33]. This is a large network divided into Nelson Bay and Tomaree zone, with more than 17,000 customers [32], [33]. The real PV power generation data is generated by incorporating the local weather data to the module, which is also predicted using ARMA and ANN techniques.

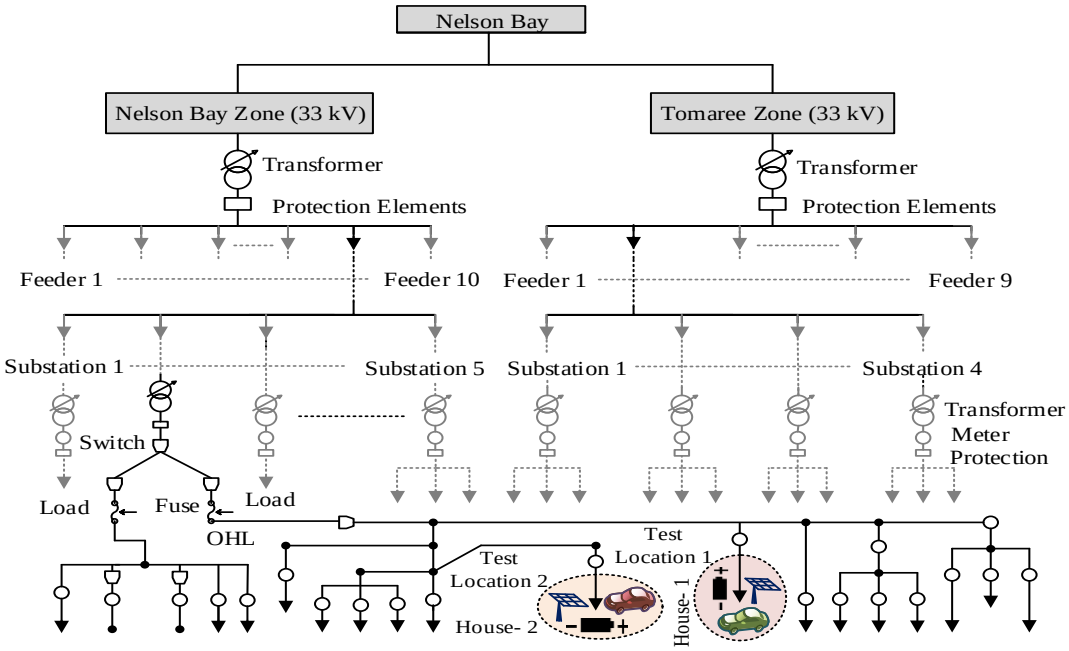

Fig. 12. Singe line diagram of the power distribution network and the test location of the proposed system.

The performance of algorithm 1 while testing at house 1 are shown in Figs. 13 and 14. Algorithm 1 is modeled based on the load profile of house 1. Fig. 14 shows the performance of house 1 when an uncertainty is added on a different time scale. The parameters used in the analysis are listed in Table I.

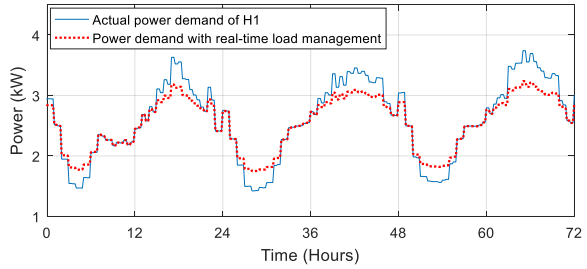

Fig. 13. The performance of the real-time energy management using algorithm 1 at H1.

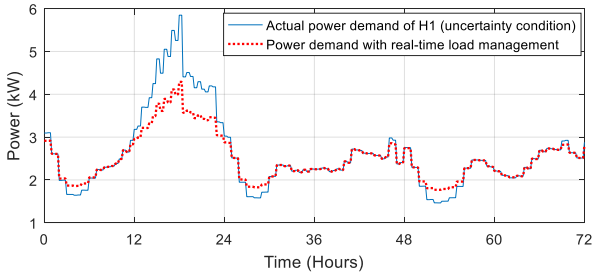

Fig. 14. Real-time energy management performance, while algorithm 1 is used and applied at H1 during uncertainty.

TABLE I

Specification of the components used in the analysis

Components	Values
Battery storage and its boundaries	$\Pi_c^b = 3\ kWh,\ \Theta_b^{min} = 40\%,\ \Theta_b^{max} = 95\%$
PV capacity	1.5 kW
EV and its bounadies	$\Pi_c^{ev} = 24\ kWh$, for V2G $\Theta_{ev}^{min} = 85\%$, $\Theta_{ev}^{max} = 95\%$

Fig. 14 shows that the real-time algorithm performs better even during uncertainty. To test their robust behavior, the same algorithm is tested at house 2 (H2) having a different load pattern, and the performance is shown in Fig. 15. Uncertainty in that different load pattern is added and the performance is shown in Fig. 16.

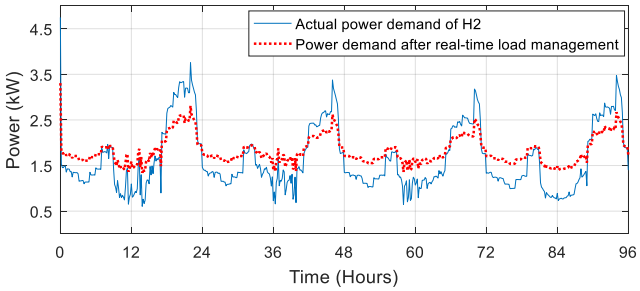

Fig. 15. Real-time energy management performance, while algorithm 1 is used and applied at H2 (which has a different load pattern).

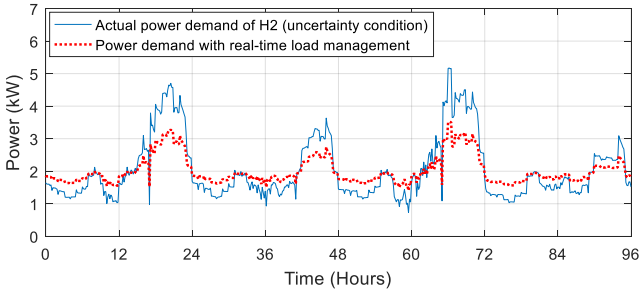

Fig. 16. Real-time energy management performance, while algorithm 1 is used and applied at H2 during uncertainty (H2 has a different load pattern).

From Figs. 15 and 16, it is clear that algorithm 1 shows a robust behavior even when applied to an unknown load pattern and during uncertain conditions. Afterwards, the ANN and ARMA prediction-based power demand management algorithm (algorithm 2 and 3) is applied at house 1 during both normal and uncertainty conditions, as shown in Figs. 17 and 18. A quantitative comparison of ANN and ARMA-based prediction and their energy management performance in compared to real-time energy management and shown in Table II.

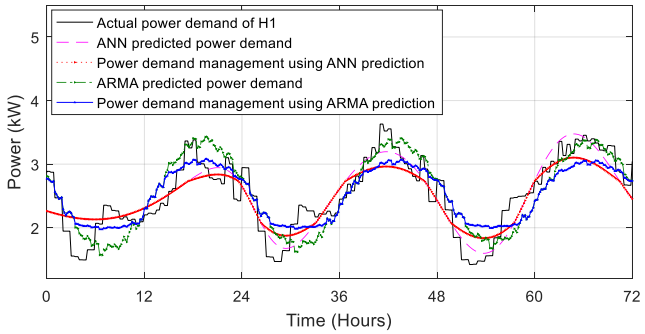

Fig. 17. Power demand management at house 1 using ANN and ARMA prediction-based techniques.

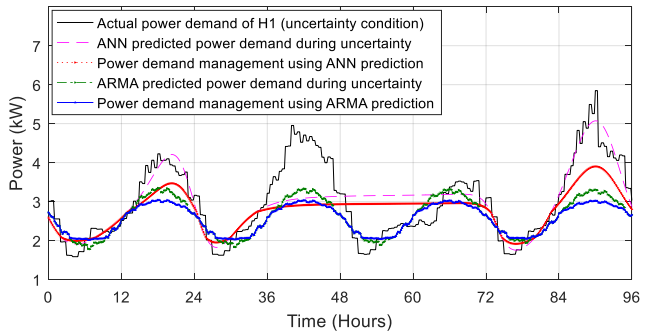

Fig. 18. Power demand management performance at house 1 during uncertainty using ANN and ARMA prediction-based techniques.

TABLE II

The performance of ANN and ARMA-based prediction, and their energy management (EM)

Observation No	Actual Load (W)	ANN Prediction (W)	ARMA prediction (W)	Real-time EM (W)	ANN-based EM (W)	ARMA-based EM (W)
1	2886.7	2256.8	2805.1	2609.5	2205.6	2768.1
2	1545.5	2149.8	1987.6	1810.5	2149.8	2058.1
3	2354.4	2136.6	1658.9	2190.8	2136.6	1992.4
4	3364.7	2698.9	3305.9	3048.6	2098.9	3018.6
5	3005.6	2875.1	3357.6	2869.1	2802.5	3044.4
6	3286.2	2885.9	3120.1	2939.7	2807.9	2925.7

From Figs. 17, 18 and Table II, it is clear that the error in prediction, i.e. the values of (α, β) dictates the amount of errors in power demand management. This error becomes severe when the load profile or PV power generation encounter any uncertainty. When (α) and (β) increases, the required power $(\mathcal{P}_r)$ from the energy resources during (t_p), and the available power $(\mathcal{P}_g)$ for charging battery storages and EV during (t_b) will mismatch. The impact of this error is further tested by applying at house 2 (H2), as shown in Figs. 19 and 20.

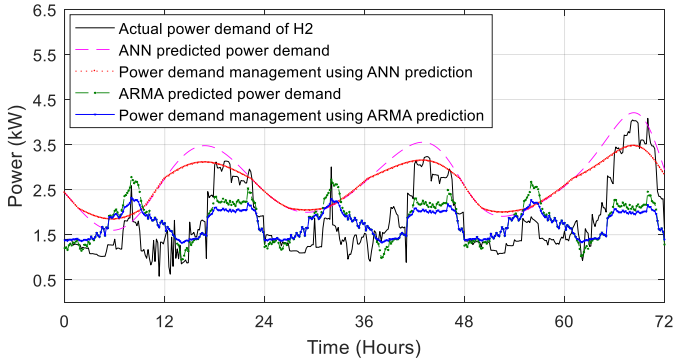

Fig. 19. ANN and ARMA prediction-based power demand management performance when tested at house 2 (different load pattern).

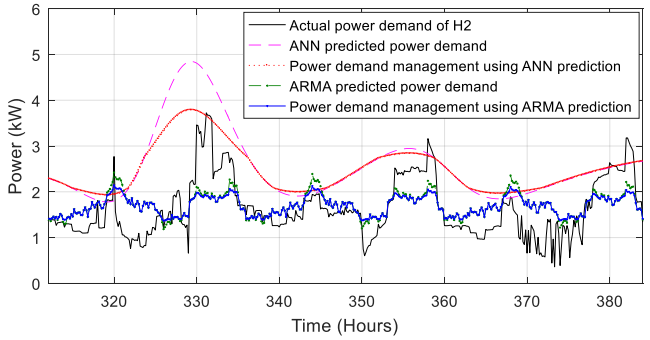

Fig. 20. ANN and ARMA prediction-based power demand management performance when tested at house 2 during uncertainty.

From Figs. 19 and 20, it is clear that the impact of prediction error becomes more severe when it is applied to an unknown network (different from the original network based on which the system is modeled). This is because the ARMA-based prediction depends on the order of AR and MA *(m, n)* which becomes untuned in an unknown network. In case of ANN, during training stage, it creates relationship between the inputs and targets, and on the new systems it works based on that relationship. The amount of prediction error and their impact on both H1 and H2 are shown in Figs. 21 and 22.

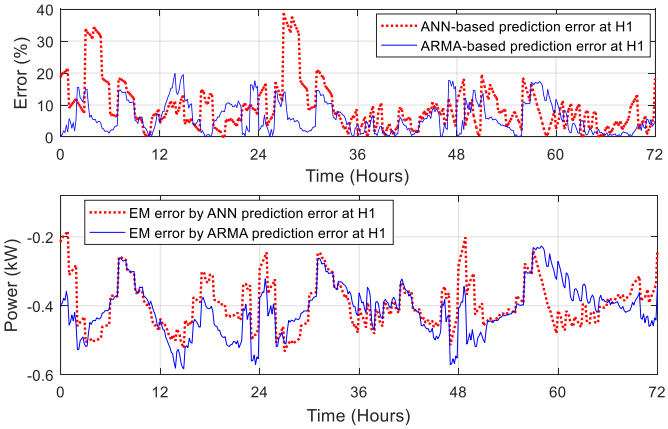

Fig. 21. The percentage of prediction error and the energy management (EM) error (in watts) during power demand management at H1.

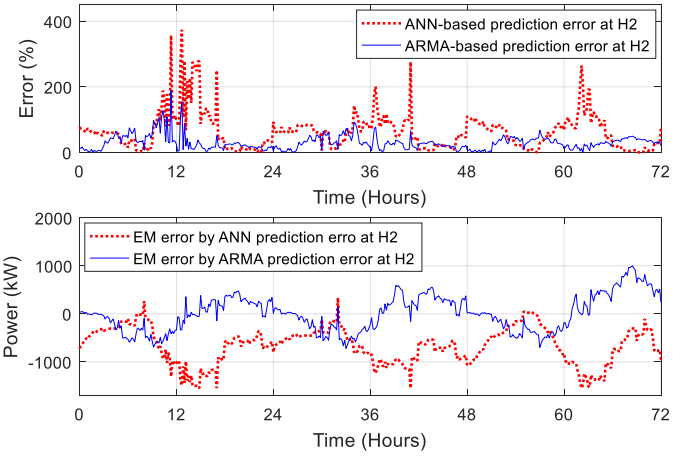

Fig. 22. The percentage of prediction error and the energy management (EM) error (in watts) during power demand management at H2.

From Figs. 21 and 22, it is clear that the ANN-based system performs better than the ARMA-based system in a known model. However, it performs worse than the ARMA-based

system in an unknown network. In most cases, the prediction error is compensated using a battery energy storage system. Therefore, in this analysis, BESSs is used to compensate for the prediction error. For a 16-day analysis at H1 for both ANN and ARMA, up to 0.38 kWh battery storage is wasted either in wrong cycling or compensating prediction error, as shown in Fig. 23. This value increases up to 0.90 kWh at H2, as shown in Fig. 24.

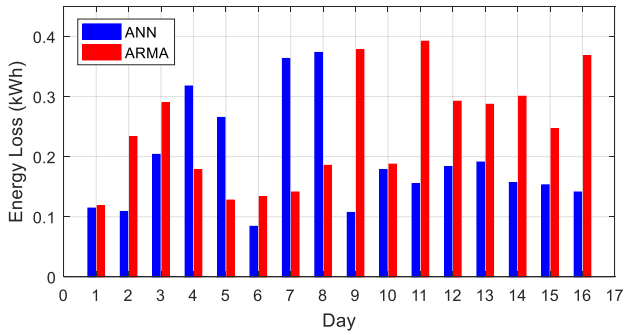

Fig. 23. kWh energy loss (error compensation energy) in each day of a 16 days analysis at H1.

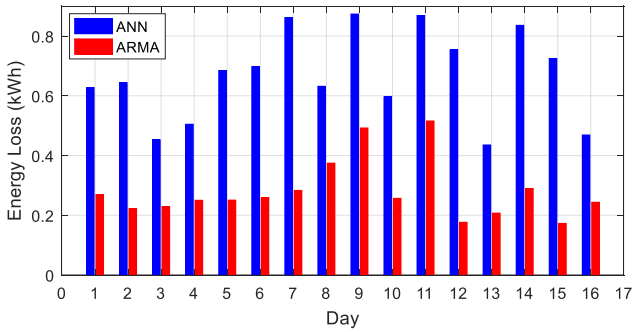

Fig. 24. kWh energy loss (error compensation energy) in each day of a 16 days analysis at H2.

A summary of the findings on prediction process is listed in Table III.

Table III. Summary of the findings on prediction errors.

Findings	Reason/description
ARMA performs better when the data pattern (trend) is similar, i.e., without having any uncertainty.	ARMA model includes the future values of its variables (maintaining a linear combination of its past observations), a constant, and a random error. So, for a regular trend or repetitive data pattern having no uncertainty, it is easier to set the model order of AR and MA model, which helps ARMA model to predict better.
The performance of an ARMA model debase when applied to a new system having uncertainty.	ARMA predicts based on the AR and MA polynomials, and it is highly dependent on the model order. So, for a new system and having unknown data trend and uncertainty, the tuning of the model order loses and degrade the prediction performance.
ANN-based prediction performs slightly better than that of an ARMA-based prediction in case of a new system.	The ANN-based model uses its past observations to map nonlinear functions and generate a time series of its future values. Unlike ARMA it is not dependent on any model order. During the training stage, it creates relationship between the inputs and targets, and on the new systems it works based on that relationship.
Higher percentage of prediction errors may cost more to consumers.	If consumer's energy management systems are dependent on predictions, any percentage of errors in prediction will enhance the chances of wrong battery storage cycling. It will degrade the battery lifetime and the EMS may not reduce the grid load demand of customers.

The investigations in Figs. 18 and 20 show that the prediction process provides a significant percentage of errors during uncertainty, which ultimately impacts the power demand management systems. As a substantial portion of appliances and energy resources of the consumers are dependent on weather conditions, consideration of environmental parameter may help the prediction and demand management systems. The case studies conducted in this section considered the real weather conditions and power networks, as shown in Fig. 12. therefore, the impact of real environmental parameters in the test location such as solar insolation, temperature and humidity on the power consumption behavior of consumers for 16 days are investigated in Figs 25 and 26. Fig. 25 shows that for the particular area like Nelson Bay, NSW, the power consumption during February and March is proportional to the temperature, i.e. the power consumption increases when the temperature increases. However, if the temperature goes too low, the power consumption behavior may show inverse relationship, because in that case the consumers may use heating systems, and which will increase the consumption. On the other hand, the humidity is inversely related to the power consumption behavior for this particular time and area.

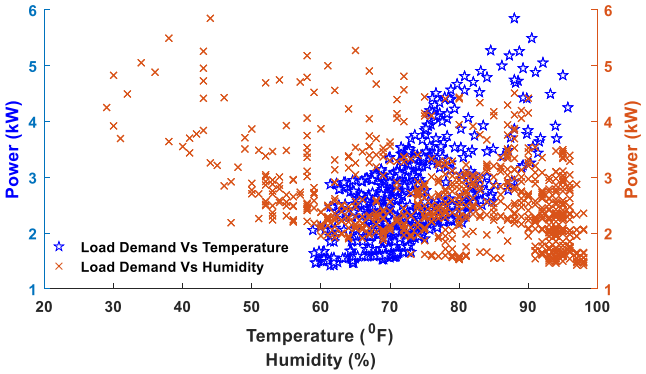

Fig. 25. Impact of weather and humidity to the energy consumption of the consumers.

The solar insolation rate also impacts the power consumption behavior. As most of the consumers have a roof-top PV, the higher the solar insolation, the more is the PV power generation, which decreases the grid's dependency of the consumers. This is evident from Fig. 26 which shows a declining trend in grid power demand of consumers with increasing solar insolation, i.e. inverse relationship.

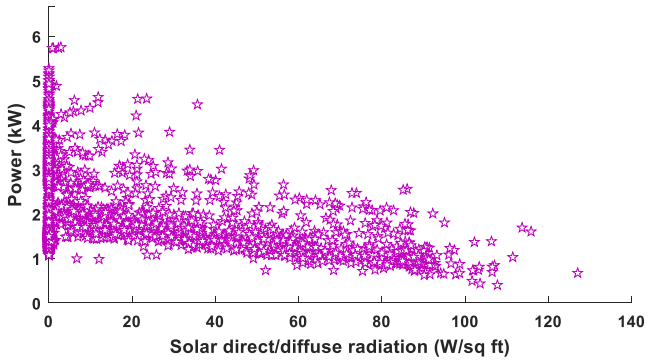

Fig. 26. Impact of solar insolation to the energy consumption of the consumers.

As the prediction errors cannot be avoided, environmental parameters (temperature, humidity and solar insolation rate) are essential to precisely identify the power demand uncertainty. Moreover, the location-specific historical data of these parameters are easily accessible, and it minimizes the need for any real-time, expensive and sophisticated data acquisition devices. The incorporation of these parameters to the demand management system can help to quickly identify the day-ahead uncertainty, take measures to meet extra power demand and avoid expensive grid electricity during peak grid uncertainty periods. Moreover, uncertainty detection can also be used to intelligently set the energy storages' (battery storage and EV) boundary conditions. As shown in Fig. 27, temperature and humidity data are used to identify the day-ahead uncertainty in the power demand and intelligently set the battery discharging setpoints. It shows that out of four days, first and last day has a significantly high-power demand, where the temperature also goes to the upper peak and humidity goes to the lower peak. Based on these parameters, the lower discharging setpoint of EV is set to 75% and the battery is set to 20% and 25% for day one and four, respectively. By using this early uncertainty detection and boundary set technique, the grid load demand can be significantly reduced.

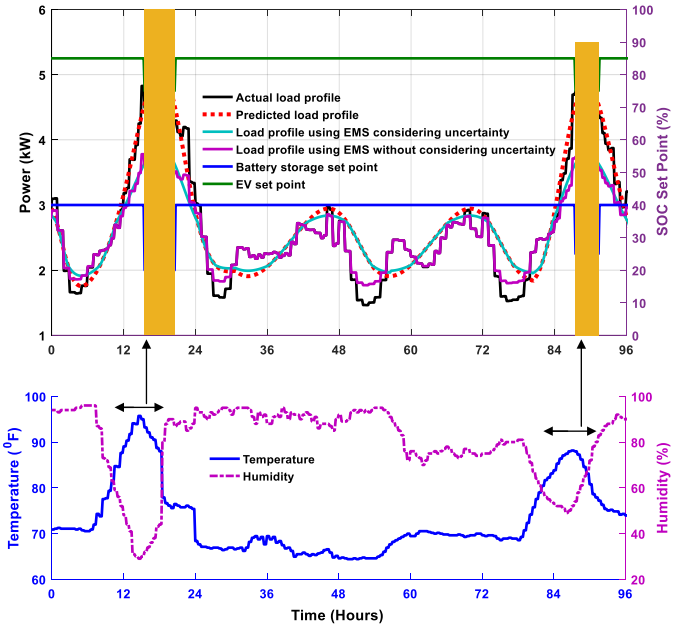

Fig. 27. Uncertainty detection and demand management considering local weather conditions.

A summary of the findings on the uncertainty detection is provided in Table IV.

Table III. Summary of the findings on uncertainty detection.

Findings	Description
An early uncertainty detection may help to minimize the grid power demand by enabling the battery storage functioning boundary change.	All the time-series based prediction techniques are dependent on its previous data history, and it degrades their performance during uncertainty. As prediction errors are unavoidable, an early detection of uncertainties may help EMS to set its energy storage's charging-discharging boundary, and it may help consumers to reduce grid dependency during high electricity costs.
Temperature has a proportional relationship with load demand (during a particular time/season)	When the temperature increases, consumers turn on their cooling devices which increase the power demand. This relationship is valid for summer season. However, if the temperature goes too low, the power consumption behavior may show inverse relationship, because in that case the consumers may use heating systems, and which will increase the consumption.
The humidity is inversely related to the power consumption behavior for a particular time and area.	Humidity sometimes dictates the human comfort factors, which may encourage customers to turn-on some devices to make their living area comfortable. However, humidity maybe highly dependent on the location, human adaptability with the weather, temperature etc. So, the inverse relation of humidity of weather may change if the location, time, consumers are changed.
Solar insolation rate is inversely related to the grid power demand of consumers having roof-top PVs.	The higher the solar insolation, the more is the PV power generation. So, the grid load demand of a consumer having roof-top PV will reduce if the solar insolation increases.

VI. Conclusion

The aim of this paper is to investigate the impact of prediction errors on the domestic peak power demand management. The study has shown that both ARMA and ANN-based techniques create errors while predicting load demand and renewable energy generation. This error becomes substantial when it is applied to a new and unknown system and faces uncertainty conditions. As a consequence, a significant amount of power demand management error is observed. The findings in various case studies suggest that a substantial capacity of battery storage is required to compensate this error, which increases battery cycling, decreases their lifecycle, and hence increases the energy cost. Moreover, the incorporation of weather information could identify the power demand uncertainties and use it for day-ahead power demand management. Future extension of this research could usefully explore the relationship between the percentage of prediction error to the electricity costs.

VII. References

[1] M. H. Rehmani, M. Reisslein, A. Rachedi, M. Erol-Kantarci, and M. Radenkovic, "Integrating Renewable Energy Resources Into the Smart Grid: Recent Developments in Information and Communication Technologies," *IEEE Trans. Ind. Informatics*, vol. 14, no. 7, pp. 2814–2825, 2018.

[2] M. Liserre, T. Sauter, and J. Y. Hung, "Future Energy Systems: Integrating Renewable Energy Sources into the Smart Power Grid Through Industrial Electronics," *IEEE Ind. Electron. Mag.*, vol. 4, no. 1, pp. 18–37, 2010.

[3] H. Turker and S. Bacha, "Optimal Minimization of Plug-in Electric Vehicle Charging Cost with Vehicle-to-Home and Vehicle-to-Grid concepts," *IEEE Trans. Veh. Technol.*, p. 1, 2018.

[4] S. A. El-Batawy and W. G. Morsi, "Optimal Design of Community Battery Energy Storage Systems With Prosumers Owning Electric Vehicles," *IEEE Trans. Ind. Informatics*, vol. 14, no. 5, pp. 1920–1931, 2018.

[5] K. Knezović, S. Martinenas, P. B. Andersen, A. Zecchino, and M. Marinelli, "Enhancing the Role of Electric Vehicles in the Power Grid: Field Validation of Multiple Ancillary Services," *IEEE Trans. Transp. Electrif.*, vol. 3, no. 1, pp. 201–209, 2017.

[6] J. Ma and X. Ma, "A review of forecasting algorithms and energy management strategies for microgrids," *Syst. Sci. Control Eng.*, vol. 6, no. 1, pp. 237–248, 2018.

[7] L. Gigoni *et al.*, "Day-Ahead Hourly Forecasting of Power Generation From Photovoltaic Plants," *IEEE Trans. Sustain. Energy*, vol. 9, no. 2, pp. 831–842, 2018.

[8] G. Li, C. Liu, C. Mattson, and J. Lawarree, "Day-Ahead Electricity Price Forecasting in a Grid Environment," *IEEE Trans. Power Syst.*, vol. 22, no. 1, pp. 266–274, 2007.

[9] F. Viani and M. Salucci, "A User Perspective Optimization Scheme for Demand-Side Energy Management," *IEEE Syst. J.*, pp. 1–4, 2018.

[10] H. Yin, C. Zhao, and C. Ma, "Decentralized Real-Time Energy Management for a Reconfigurable Multiple-Source Energy System," *IEEE Trans. Ind. Informatics*, vol. 14, no. 9, pp. 4128–4137, 2018.

[11] S. G. Faddel and O. A. Mohammed, "Automated Distributed Electric Vehicle Controller for Residential Demand Side Management," *IEEE Trans. Ind. Appl.*, p. 1, 2018.

[12] Y. Yang, H. Li, A. Aichhorn, J. Zheng, and M. Greenleaf, "Sizing Strategy of Distributed Battery Storage System With High Penetration of Photovoltaic for Voltage Regulation and Peak Load Shaving," *IEEE Trans. Smart Grid*, vol. 5, no. 2, pp. 982–991, 2014.

[13] K. Mahmud, M. J. Hossain, and J. Ravishankar, "Peak-Load Management in Commercial Systems With Electric Vehicles," *IEEE Syst. J.*, vol. 13, no. 2, pp. 1872–1882, 2019.

[14] Z. Liu, Q. Wu, M. Shahidehpour, C. Li, S. Huang, and W. Wei, "Transactive Real-time Electric Vehicle Charging Management for Commercial Buildings with PV On-site Generation," *IEEE Trans. Smart Grid*, p. 1, 2018.

[15] M. O. Badawy and Y. Sozer, "Power Flow Management of a Grid Tied PV-Battery System for Electric Vehicles Charging," *IEEE Trans. Ind. Appl.*, vol. 53, no. 2, pp. 1347–1357, 2017.

[16] C. C. Lin, D. J. Deng, W. Y. Liu, and L. Chen, "Peak Load Shifting in the Internet of Energy With Energy Trading Among End-Users," *IEEE Access*, vol. 5, pp. 1967–1976, 2017.

[17] Q. Xu, Y. Ding, Q. Yan, A. Zheng, and P. Du, "Day-Ahead Load Peak Shedding/Shifting Scheme Based on Potential Load Values Utilization: Theory and Practice of Policy-Driven Demand Response in China," *IEEE Access*, vol. 5, pp. 22892–22901, 2017.

[18] W. Su, J. Wang, and J. Roh, "Stochastic Energy Scheduling in Microgrids With Intermittent Renewable Energy Resources," *IEEE Trans. Smart Grid*, vol. 5, no. 4, pp. 1876–1883, 2014.

[19] K. Mahmud, M. S. Rahman, J. Ravishankar, M. Hossain, and J. M. Guerrero, "Real-Time Load and Ancillary Support for a Remote Island Power System Using Electric Boats," *IEEE Trans. Ind. Informatics*, 2019.

[20] P. Su *et al.*, "Recent Trends in Load Forecasting Technology for the Operation Optimization of Distributed Energy System," *Energies*, vol. 10, no. 9, p. 1303, 2017.

[21] A. K. Singh, S. Khatoon, M. Muazzam, and D. K. Chaturvedi, "Load forecasting techniques and methodologies: A review," in *Power, Control and Embedded Systems (ICPCES), 2012 2nd International Conference on*, 2012, pp. 1–10.

[22] J. C. López, M. J. Rider, and Q. Wu, "Parsimonious Short-Term Load Forecasting for Optimal Operation Planning of Electrical Distribution Systems," *IEEE Trans. Power Syst.*, p. 1, 2018.

[23] J. F. M. Pessanha and N. Leon, "Long-term forecasting of household and residential electric customers in Brazil," *IEEE Lat. Am. Trans.*, vol. 10, no. 2, pp. 1537–1543, 2012.

[24] A. Y. Alanis, "Electricity Prices Forecasting using Artificial Neural Networks," *IEEE Lat. Am. Trans.*, vol. 16, no. 1, pp. 105–111, 2018.

[25] S. Ghosh, S. Rahman, and M. Pipattanasomporn, "Distribution Voltage Regulation Through Active Power Curtailment With PV Inverters and Solar Generation Forecasts," *IEEE Trans. Sustain. Energy*, vol. 8, no. 1, pp. 13–22, 2017.

[26] E. A. Feinberg and D. Genethliou, "Load forecasting," in *Applied mathematics for restructured electric power systems*, Springer, 2005, pp. 269–285.

[27] A. Tascikaraoglu, O. Erdinc, M. Uzunoglu, and A. Karakas, "An adaptive load dispatching and forecasting strategy for a virtual power plant including renewable energy conversion units," *Appl. Energy*, vol. 119, pp. 445–453, 2014.

[28] K. Mahmud, A. K. Sahoo, J. Ravishankar, and Z. Dong, "Coordinated Multilayer Control for Energy Management of Grid-Connected AC Microgrids," *IEEE Trans. Ind. Appl.*, 2019.

[29] H. Wu, M. Shahidehpour, and A. Al-Abdulwahab, "Hourly demand response in day-ahead scheduling for managing the variability of renewable energy," *IET Gener. Transm. Distrib.*, vol. 7, no. 3, pp. 226–234, 2013.

[30] C. Chen, S. Duan, T. Cai, B. Liu, and G. Hu, "Smart energy management system for optimal microgrid economic operation," *IET Renew. power Gener.*, vol. 5, no. 3, pp. 258–267, 2011.

[31] H. Kanchev, D. Lu, F. Colas, V. Lazarov, and B. Francois, "Energy management and operational planning of a microgrid with a PV-based active generator for smart grid applications," *IEEE Trans. Ind. Electron.*, vol. 58, no. 10, pp. 4583–4592, 2011.

[32] "Customer Applications: SGSC Technical Compendium," Sydney, Australia.

[33] "DGDS214-Customer Grade Distribution Storage Optimize Distribution Generation—A Grid PS+EDGE Modeling Platform Case Study," Australia.